JACS
JOURNAL OF THE AMERICAN CHEMICAL SOCIETY
Article
Cite This: J. Am. Chem. Soc. 2019, 141, 10924−10929
pubs.acs.org/JACS

Metal−Organic Framework Coating Enhances the Performance of Cu_2O in Photoelectrochemical CO_2 Reduction

Xi Deng,[†,∥] Rui Li,[†,‡,∥] Sikai Wu,[†,§,∥] Li Wang,[†] Jiahua Hu,[†] Jun Ma,[†] Wenbin Jiang,[†] Ning Zhang,[†] Xusheng Zheng,[†] Chao Gao,*[,†] Linjun Wang,[†] Qun Zhang,*[,†] Junfa Zhu,[†] and Yujie Xiong*[,†]

[†]Hefei National Laboratory for Physical Sciences at the Microscale, Collaborative Innovation Center of Chemistry for Energy Materials (iChEM), School of Chemistry and Materials Science, and National Synchrotron Radiation Laboratory, University of Science and Technology of China, Hefei, Anhui 230026, China

[‡]School of Mechanical and Aerospace Engineering, Nanyang Technological University, Singapore 639798, Singapore

[§]Department of Chemistry, Pennsylvania State University, University Park, Pennsylvania 16802, United States

Supporting Information

ABSTRACT: Photoelectrochemical (PEC) reduction of CO_2 into chemical fuels and chemical building blocks is a promising strategy for addressing the energy and environmental challenges, which relies on the development of p-type photocathodes. Cu_2O is such a p-type semiconductor for photocathodes but commonly suffers from detrimental photocorrosion and chemical changes. In this communication, we develop a facile procedure for coating a metal−organic framework (MOF) on the surface of a Cu_2O photocathode, which can both prevent photocorrosion and offer active sites for CO_2 reduction. As evidenced by ultrafast spectroscopy, the formed interface can effectively promote charge separation and transfer. As a result, both the activity and durability of Cu_2O are dramatically enhanced for PEC CO_2 reduction. This work provides fresh insights into the design of advanced hybrid photoelectrodes and highlights the important role of interfacial charge dynamics in PEC CO_2 conversion.

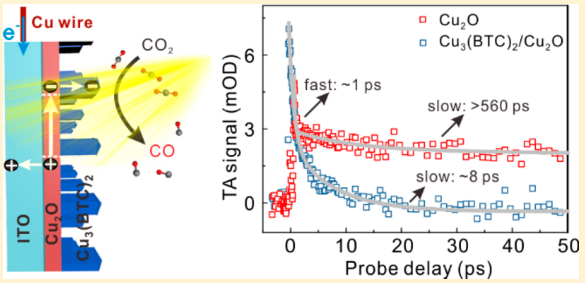

INTRODUCTION

Direct conversion of CO_2 into storable value-added chemical fuels and chemical building blocks is gaining increasing attention.[1−5] Among various approaches, photoelectrochemical (PEC) CO_2 conversion that combines together the merits of both electrocatalysis and photocatalysis is one of the most promising yet challenging strategies.[6−14] Typically, such a PEC system utilizes a p-type semiconductor as a photocathode to perform CO_2 reduction; however, the choice of p-type semiconductors harvesting visible light is quite limited. Cuprous oxide (Cu_2O) is a p-type semiconductor with high carrier mobility, sufficient Cu active sites for CO_2 activation, broad absorption of visible light, low toxicity, and high natural abundance,[11,12] rendering it a promising candidate for PEC CO_2 reduction.

The practical application of a Cu_2O photocathode is yet limited by the fact that it suffers from detrimental photocorrosion and its Cu active sites undergo chemical changes during catalytic reactions under an external potential.[15,16] Surface coating with metal oxide can efficiently help prevent the photocorrosion of Cu_2O,[17] which however usually relies on expensive atomic layer deposition and lacks effective catalytic sites. Ideally, a surface coating material should not only improve the photostability of a Cu_2O photocathode but also offer the catalytic sites that can efficiently receive photoexcited electrons from the photocathode for CO_2 activation. Metal−organic frameworks (MOFs) are a class of porous materials that can be facilely coated on inorganic materials and offer active sites for various catalytic reactions.[18,19] We have previously demonstrated that photogenerated electrons can effectively transfer from a semiconductor to a MOF for CO_2 reduction.[20] Such promising features would make the MOF material an ideal candidate for surface coating on a Cu_2O photocathode to achieve enhanced PEC CO_2 reduction.

Herein, we report a facile procedure for coating a MOF on the surface of a Cu_2O photocathode to enhance activity and durability in PEC CO_2 reduction. Ultrafast spectroscopy demonstrates that an ideal interface is built to facilitate the electron transfer from a Cu_2O substrate to a surface MOF layer. In our approach, the coated MOF layer plays multiple roles in PEC CO_2 reduction, i.e., protecting underlying Cu_2O from photocorrosion, facilitating electron transfer, and offering active sites for CO_2 reduction. As a proof of concept, $Cu_3(BTC)_2$ (BTC = benzene-1,3,5-tricarboxylate, named HKUST-1 in the literature) is selected as the MOF model, as it can provide Cu sites for CO_2 activation. Given that copper-based MOF is unstable in aqueous solution,[21,22] PEC

Received: June 11, 2019
Published: June 14, 2019

DOI: 10.1021/jacs.9b06239
J. Am. Chem. Soc. 2019, 141, 10924−10929

CO_2 reduction is performed in acetonitrile—a typical solvent for homogeneous electrocatalysts. Encouragingly, the designed hybrid MOF/Cu_2O structure exhibits a prominently enhanced performance compared with Cu_2O in PEC reduction of CO_2 to CO. CO is an important chemical building block that can be transformed into virtually any carbon-based fuels and chemicals through the Fischer–Tropsch and gas-to-methanol processes.[8] The present work would offer a promising approach to designing, fabricating, and modifying photoelectrodes for CO_2 conversion and utilization through PEC.

EXPERIMENTAL SECTION

Fabrication of Photoelectrodes. Cu_2O thin films were electrodeposited on indium tin oxide (ITO) glass in a three-electrode system, which contained a platinum foil as a counter electrode, a saturated calomel electrode (SCE) as a reference electrode, and ITO glass as a working electrode. The solution for Cu_2O electrodeposition contained 0.4 M $CuSO_4$ and 4 M lactic acid in deionized water and was maintained at 60 °C. The pH was adjusted to 10.5 by the addition of 4 M NaOH solution. After the electrodeposition, the Cu_2O/ITO was rinsed by deionized water and ethanol several times and then dried under nitrogen. To fabricate $Cu_3(BTC)_2/Cu_2O$/ITO, the Cu_2O/ITO was then immersed in a DMF solution of H_3BTC (0.01 M, 40 mL), which was maintained at 70 °C for 40 min in a three-necked round-bottom flask. Subsequently, the $Cu_3(BTC)_2/Cu_2O$/ITO was obtained and rinsed by ethanol several times and then dried under nitrogen.

Ultrafast Spectroscopy Characterizations. The femtosecond transient absorption data were recorded on a modified pump–probe spectrometer (ExciPro, CDP) in combination with an ultrafast amplified laser system (Coherent). All of the measurements were performed under ambient conditions. The strong pump laser (pulse duration ~35 fs; pulse energy ~10 μJ at the sample cell) with a center wavelength at 480 nm was used to examine the samples. The weak probe pulses (<1 μJ/pulse) were provided by a stable white-light continuum. The time delays between the pump and probe pulses were varied by a motorized optical delay line (minimum step, 1.56 fs; maximum delay, ~3.0 ns). The spectral and temporal profiles of the pump-induced transient absorbance changes were visualized by a 1024-pixel imaging spectrometer (CDP2022i) and further processed by ExiPro 2.6 software.

SRPES Characterization. Synchrotron-radiation photoemission spectroscopy (SRPES) experiments were performed at the Photoemission Endstation (BL10B) in National Synchrotron Radiation Laboratory (NSRL), China. The valence-band spectra were measured using synchrotron-radiation light as the excitation source with a photon energy of 168.84 eV and referenced to the Fermi level (E_F = 0) determined from Au. The work function (Φ) was determined by the difference between the photon energy and the width of whole valence-band spectra. A sample bias of −10 V was applied for the secondary electron cutoff.

Photoelectrochemical Measurements. Photoelectrochemical (PEC) experiments were carried out in an airtight, online three-electrode quartz photoelectrochemical cell (Perfect Light, China) under irradiation, coupled with an electrochemical workstation and a gas chromatograph (GC). The PEC system containing a platinum foil as a counter electrode, Ag/Ag^+ as a reference electrode with a ferrocene/ferrocenium (Fc/Fc^+) couple as an internal potential reference, and an as-fabricated photocathode as a working electrode was investigated in CO_2-saturated acetonitrile containing 0.1 M tetrabutylammonium hexafluorophosphate as a supporting electrolyte and was irradiated under a 300 W xenon lamp with a 420 nm long-wave-pass cutoff filter (i.e., λ > 420 nm) or an AM 1.5G filter. The power density was measured to be 254 mW·cm^{-2} with a λ > 420 nm cutoff filter and 100 mW·cm^{-2} with an AM 1.5G filter, respectively. The illuminated area was 2.5 cm^{-2}. As the Ag/Ag^+ electrode is not a standard reference for a nonaqueous system, the recorded potentials vs Ag/Ag^+ were converted to the ones vs Fc/Fc^+ by the following equation: E(vs Fc/Fc^+) = E(vs Ag/Ag^+) − E(Fc/Fc^+), where the Fc/Fc^+ potential vs Ag/Ag^+ is measured as 0.19 V in acetonitrile.[23] The entire reaction setup was vacuum degassed, and then, the high-purity CO_2 gas was filled into the reaction setup to reach a pressure of 1 bar. The amounts of CO evolved were determined using a gas chromatograph (GC, Techcomp GC-7900, China) equipped with a TDX-01 packed column. CO was converted to CH_4 by a methanation reactor and then analyzed by a flame ionization detector (FID). The isotope-labeled experiments were performed using $^{13}CO_2$ instead of $^{12}CO_2$, and the products were analyzed using gas chromatography–mass spectrometry (GC-MS, 7890A and 5975C, Agilent).

Faradaic efficiency (FE) was calculated by the following equation[8]

$$\mathrm{FE} = \frac{2 \times n_{\mathrm{CO}} \times F}{Q}$$

where 2 is the number of needed electrons for CO evolution, n_{CO} is the molar number of CO products, F is the Faraday constant, and Q is the total passed charge. Solar-to-CO (STC) efficiency was calculated according to the following equation[8]

$$\mathrm{STC}\% = \frac{|J\ (\mathrm{mA\ cm^{-2}})| \times \mathrm{FE}\ (\%) \times |(1.34 - |E|)\ (\mathrm{V})|}{P\ (\mathrm{mW\ cm^{-2}})}$$

where J is the photocurrent density, FE is the Faradaic efficiency toward CO, E is the applied potential vs RHE, P is the light power density, and 1.34 V is the thermodynamic potential for CO_2 reduction to CO at 25 °C. Incident-photon-to-current conversion efficiency (IPCE) data were collected on a Newport electrochemical station with a solar simulator (Newport 66984), coupled with a filter (Newport 74010) and aligned monochromator (Newport 74125).

RESULTS AND DISCUSSION

Figure 1 illustrates the setup of our PEC CO_2 reduction system where the photocathode contains column-like $Cu_3(BTC)_2$

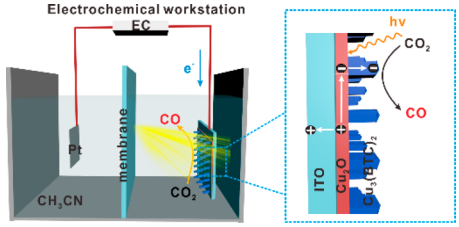

Figure 1. Schematic illustration for PEC CO_2 reduction in acetonitrile using a hybrid Cu-MOF/Cu_2O photocathode (unscaled).

MOF structures on the Cu_2O film surface. Such a photocathode is formed by first electrodepositing Cu_2O thin film on indium tin oxide (ITO) glass, followed by the growth of $Cu_3(BTC)_2$ with Cu_2O as a copper precursor via solution-phase reactions. While X-ray diffraction characterization indicates that our synthetic method typically coats the Cu_2O surface with crystalline $Cu_3(BTC)_2$ (Figures S1 and S2), the as-fabricated photocathode is further characterized by Fourier transform-infrared (FT-IR) spectroscopy. Figure 2a displays the absorption bands ranging from 1700 to 1300 cm^{-1} that can be ascribed to the vibrations of BTC linker molecules.[19,24] Furthermore, the two additional significant peaks in reference to Cu_2O at 730 and 760 cm^{-1} are assigned to the bonding of Cu with BTC linker molecules, indicating the metal–organic coordination state of $Cu_3(BTC)_2$. The formation of $Cu_3(BTC)_2$ on the Cu_2O surface is further confirmed by Raman spectroscopy (Figure 2b). While the four peaks at 218, 415, 527, and 631 cm^{-1} are ascribed to Cu_2O,[11] the additional peaks between 700 and 1620 cm^{-1} correspond to the

DOI: 10.1021/jacs.9b06239
J. Am. Chem. Soc. 2019, 141, 10924–10929

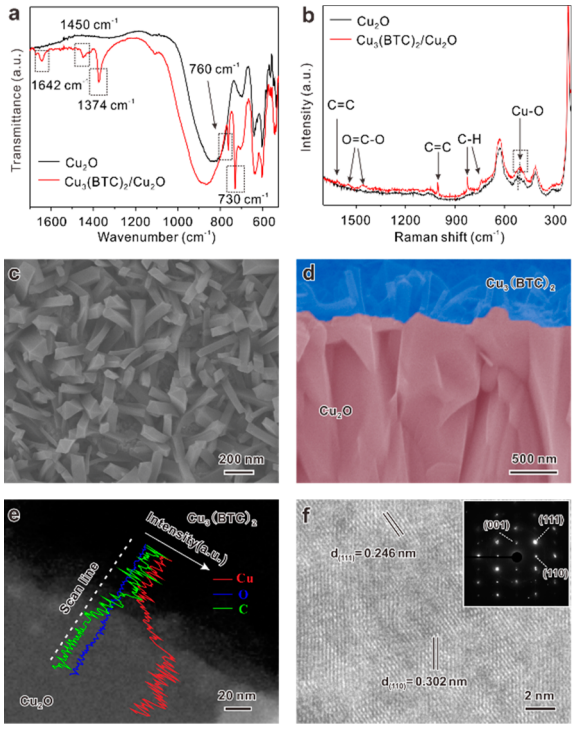

Figure 2. (a) FT-IR and (b) Raman spectra of $Cu_3(BTC)_2/Cu_2O$ and Cu_2O photocathodes. (c) Top-view and (d) cross-section SEM images of $Cu_3(BTC)_2/Cu_2O$. (e) TEM image and EDS line scan profiles of a sliced $Cu_3(BTC)_2/Cu_2O$ cross section. (f) HRTEM image and SEAD pattern (inset) taken at Cu_2O in the sliced $Cu_3(BTC)_2/Cu_2O$.

characteristic Raman active vibration modes of BTC linker molecules.[25] The shifted peak at 504 cm^{-1} for $Cu_3(BTC)_2/Cu_2O$ is ascribed to the vibration of the Cu−O coordination bond, suggesting the metal−organic coordination in $Cu_3(BTC)_2$. Taken together with X-ray photoelectron spectroscopy (XPS) (Figure S3), the data prove that a hybrid structure composed of two materials—Cu_2O and $Cu_3(BTC)_2$—has been formed on the photocathode.

Upon acquiring the overall composition information, we further examine the interface between Cu_2O and $Cu_3(BTC)_2$—the key to interfacial electron transfer in PEC reduction. While the Cu_2O thin film on ITO is mainly composed of small crystals in a sharp pyramid shape (Figure S4), $Cu_3(BTC)_2$ MOF structures grow from the Cu_2O surface into some standing-out columns with an average diameter of 100 nm and a length of about 400 nm, as indicated by scanning electron microscopy (SEM) (Figure 2c and d). Although energy-dispersive X-ray spectroscopy (EDS) by SEM roughly reveals the composition distribution in different regions (Figures S5 and S6), it can hardly resolve the interface between Cu_2O and $Cu_3(BTC)_2$. For this reason, we mill the photocathode into a slice through a focused ion beam (FIB), which then can be imaged by transmission electron microscopy (TEM). EDS line scan and mapping across the interface (Figures 2e and S7) reveal that the contents of Cu and C are more concentrated at one side of the region, while O spans the entire region. This confirms the heterogeneous nature of the interface. High-resolution TEM (HRTEM) further resolves the lattice fringes with spacings of 0.246 and 0.302 nm in the Cu_2O region (Figure 2f), which can be assigned to the (111) and (110) planes of Cu_2O, respectively, in agreement with the selected area electron diffraction (SAED) pattern (inset of Figure 2f).[15,26,27] Note that $Cu_3(BTC)_2$ is not very stable under a high-energy electron beam so that we are unable to observe lattice fringes from $Cu_3(BTC)_2$ on the branched-out column.

The formed $Cu_3(BTC)_2/Cu_2O$ interface would enable charge transfer between the Cu_2O semiconductor and the $Cu_3(BTC)_2$ MOF upon photoexcitation, whose direction depends on their band structures. It turns out that $Cu_3(BTC)_2$ coating does not alter the bandgap of Cu_2O, while it is optically transparent to ensure the light absorption of Cu_2O (Figure S8). To resolve the band structures, we collect synchrotron radiation photoemission spectroscopy (SRPES) on Cu_2O and $Cu_3(BTC)_2$ (Figure S9). As illustrated in Figure 3a, the conduction band minimum (CBM) and

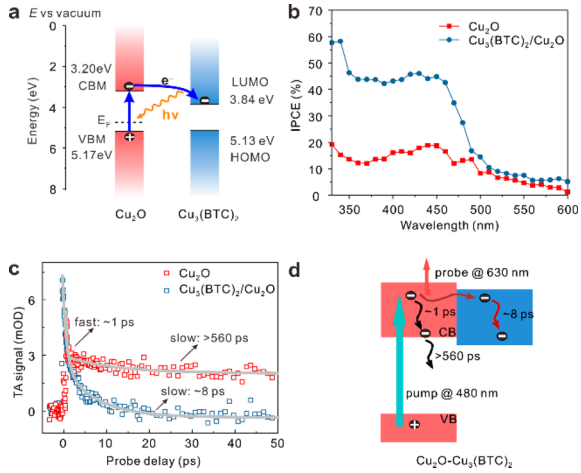

Figure 3. (a) Schematic energy-level diagram showing the electron transfer from Cu_2O to $Cu_3(BTC)_2$. E_F: Fermi level. (b) Wavelength-dependent IPCE of Cu_2O and $Cu_3(BTC)_2/Cu_2O$ at −0.97 V vs RHE. (c) Ultrafast transient absorption as a function of probe delay for Cu_2O and $Cu_3(BTC)_2/Cu_2O$ (pump at 480 nm; probe at 630 nm). The time constants are derived from a biexponential fitting. (d) Schematic illustration for the involved photoexcited electron dynamics.

valence band maximum (VBM) of Cu_2O relative to the vacuum level are determined to be 3.20 and 5.17 eV, respectively. Meanwhile, the lowest unoccupied molecular orbital (LUMO) and highest occupied molecular orbital (HOMO) energy levels of $Cu_3(BTC)_2$ are measured as 3.84 and 5.13 eV, respectively. Both band structures agree well with the published results.[28,29] Since the LUMO of $Cu_3(BTC)_2$ is lower than the CBM of Cu_2O, the photoexcited electrons in the conduction band (CB) of Cu_2O can be preferentially transferred to the LUMO of $Cu_3(BTC)_2$, enabling subsequent CO_2 reduction. Incident-photon-to-current-conversion efficiency (IPCE, Figure 3b) reveals that $Cu_3(BTC)_2$ coating can significantly facilitate the photogenerated charge separation and transfer in Cu_2O, as verified also by photocurrents and electrochemical impedance spectroscopy (Figure S10).

To further elucidate the key role of $Cu_3(BTC)_2$ in charge separation and transfer, we interrogate the electron dynamics involved in the systems by means of ultrafast transient absorption (TA) spectroscopy. As shown in Figure 3c, the positive-value photoinduced absorption signal for bare Cu_2O builds up within the instrument response function (ca. 100 fs) of our pump−probe measurements (pump at 480 nm; probe at

DOI: 10.1021/jacs.9b06239
J. Am. Chem. Soc. 2019, 141, 10924−10929

630 nm) and then decays in about 1 ps, followed by a long-time recovery (>560 ps). As schematically illustrated in Figure 3d, the first decay reflects the instantaneous electron relaxation within the CB of Cu_2O due to the electron−phonon scattering effect, while the subsequent long-time recovery corresponds to the undesired electron−hole recombination. In stark contrast, once Cu_2O is interfaced with $Cu_3(BTC)_2$, such an eventual recovery becomes much faster (ca. 8 ps). This observation can be understood as follows. In competition with the relaxation within the CB of Cu_2O, the photoexcited electrons preferentially transfer to the adjacent interface states formed between Cu_2O and $Cu_3(BTC)_2$ within 1 ps and then undergo recovery within such interface states in a rather prompt manner (sub-10 ps). Evidently, the alteration of electron dynamics indicates that coating of $Cu_3(BTC)_2$ on the Cu_2O surface leads to a preferential channelling of the photogenerated electrons to reach the MOF component of the hybrid system, significantly improving the efficiency of electron−hole separation therein.

Upon tracing the charge dynamics, we are now in a position to examine the performance of $Cu_3(BTC)_2/Cu_2O$/ITO as a photocathode for PEC CO_2 reduction without any sacrificial agent. The PEC performance is assessed in CO_2-saturated acetonitrile containing 0.1 M tetrabutylammonium hexafluorophosphate ($TBAPF_6$) as a supporting electrolyte with an online three-electrode quartz PEC cell (Figure S11). Figure 4a shows the production yields of CO by $Cu_3(BTC)_2/Cu_2O$/ITO in reference to Cu_2O/ITO. In the dark, the production yields of CO increase with the applied potentials for both $Cu_3(BTC)_2/Cu_2O$ and Cu_2O, but the yields for $Cu_3(BTC)_2/Cu_2O$ are about 2 times higher than those for Cu_2O. This indicates that $Cu_3(BTC)_2$ can provide effective catalytic sites for the reduction of CO_2 molecules to CO. When the system is switched to visible light irradiation, the yields for $Cu_3(BTC)_2/Cu_2O$ are obviously enhanced by about 4 times. This observation verifies again that the photogenerated electrons on Cu_2O can preferentially transfer to $Cu_3(BTC)_2$ and contribute to the significant enhancement on CO_2 reduction. Notably, the low performance of bare Cu_2O under visible light irradiation is caused by photocorrosion. Note that it is not feasible to compare the applied potential here in a nonaqueous system with that typically in aqueous solvent; however, the applied potential in our work is substantially lower than that in the same nonaqueous solvent.[12] To trace the carbon source of produced CO, we perform PEC CO_2 reduction using a ^{13}C isotopic label whose products are identified by gas chromatography−mass spectrometry (GC−MS, Figure 4b). The GC peak appearing at 1.8 min with the m/z = 29 in MS is assigned to the generated ^{13}CO, confirming that the produced CO indeed originates from CO_2. In the meantime, no liquid hydrocarbon and other gas products derived from CO_2 can be detected.

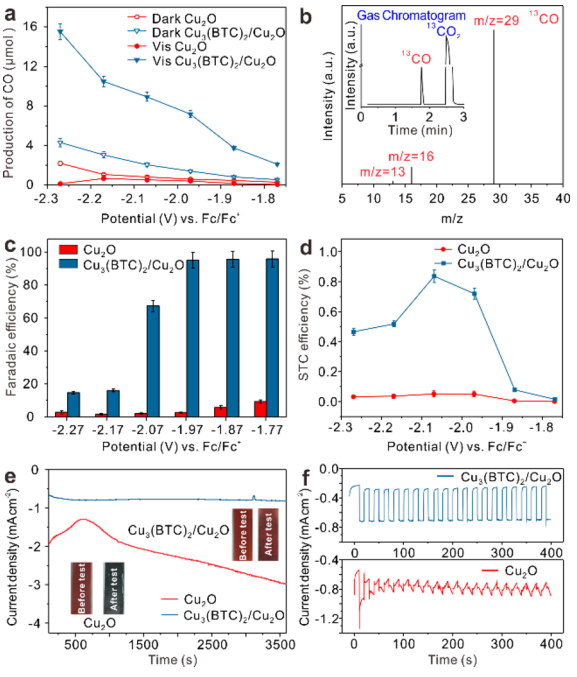

Figure 4. (a) Production yields of CO for 1 h under visible light (λ > 420 nm) irradiation and in the dark using Cu_2O/ITO or $Cu_3(BTC)_2/Cu_2O$/ITO as a photocathode. (b) GC-MS analysis of carbon products in PEC $^{13}CO_2$ reduction using $Cu_3(BTC)_2/Cu_2O$/ITO. (c) Faradaic efficiencies of CO production for 1 h in the dark and (d) solar-to-CO (STC) efficiencies for 1 h under AM 1.5G illumination by Cu_2O/ITO and $Cu_3(BTC)_2/Cu_2O$/ITO as a function of potentials. Chronoamperometry I−t curves of the Cu_2O/ITO and $Cu_3(BTC)_2/Cu_2O$/ITO photocathodes at a constant potential of −1.97 V vs Fc/Fc$^+$: (e) under constant visible light irradiation during a PEC CO_2 reduction measurement and (f) under chopped visible light in the presence of CO_2. The insets in panel e are the photographs of the corresponding photocathodes.

To prove the efficacy of Cu atoms in $Cu_3(BTC)_2$ as catalytic sites, we measure the Faradaic efficiencies (FEs) of our $Cu_3(BTC)_2/Cu_2O$/ITO electrode in the dark. As displayed in Figure 4c, the CO production on $Cu_3(BTC)_2/Cu_2O$ at applied potentials between −1.77 and −1.97 V vs Fc/Fc$^+$ reaches high FEs of about 95%, well exceeding the performance of a bare Cu_2O electrode and the state-of-the-art dark electrocatalysts for CO_2 reduction to CO under identical acetonitrile/$TBAPF_6$ conditions (Table S1). It is believed that the defect sites in $Cu_3(BTC)_2$ provide coordinatively unsaturated Cu sites for the reduction of CO_2 to CO (Figure S12). At a more negative bias, a decrease in FEs can be observed for both electrodes, as CO_2 mass transport is too limited to match electron supply and Cu_2O is reduced to a certain level. The excessive transformation of Cu_2O to Cu(0) on the surface would destroy the interface between Cu_2O and $Cu_3(BTC)_2$ (which holds the key to efficient electron transfer to the active sites provided by $Cu_3(BTC)_2$, as proven in Figure 3). We further evaluate solar-to-CO (STC) efficiency under AM 1.5G illumination (Figure 4d). The STC efficiency of our $Cu_3(BTC)_2/Cu_2O$/ITO photocathode reaches 0.83% at −2.07 V vs Fc/Fc$^+$, comparable to the benchmark photocathodes (0.87%).[8] Note that the effects of $Cu_3(BTC)_2$ amount and Cu_2O thickness on PEC CO_2 reduction have been optimized for maximally enhancing PEC CO_2 reduction performance (Figures S13−S15).

Given that $Cu_3(BTC)_2$ has enhanced the PEC activity of the Cu_2O photocathode, we further assess photocathode stability—a typical bottleneck for Cu_2O material. The chronoamperometry I−t curves of the $Cu_3(BTC)_2/Cu_2O$/ITO photocathode show a nearly constant current density under visible light in PEC CO_2 reduction (Figure 4e) as well as a steady photocurrent density under chopped visible light (Figure 4f). In comparison, unstable current density is observed for the Cu_2O/ITO photocathode under continuous illumination, while photocurrent exhibits a fast decay during the illumination. This indicates that the $Cu_3(BTC)_2$ coating greatly enhances the photostability of the Cu_2O photocathode

DOI: 10.1021/jacs.9b06239
J. Am. Chem. Soc. 2019, 141, 10924−10929

indeed. The time-dependence FEs and STC efficiencies for CO production as well as long-term chronoamperometry $I-t$ curves further confirm the durability of our $Cu_3(BTC)_2/Cu_2O$/ITO photocathode (Figure S16).

We also examine the photocathodes after PEC reactions with the aid of SEM, XPS, XRD, and FT-IR (Figures S17–S19). The $Cu_3(BTC)_2/Cu_2O$ undergoes no significant change but slight electrochemical reduction. As such, the dark current by $Cu_3(BTC)_2/Cu_2O$/ITO in the presence of CO_2 in Figure 4f should mainly originate from the reduction of CO_2 molecules to CO, which has been evidenced by the CO_2 reduction in the dark in Figure 4a. In comparison, the characterizations (Figure S18) reveal that the Cu_2O suffers from severe photocorrosion oxidation (also indicated by the color change to black, inset in Figure 4e) as well as slight electrochemical reduction. The severe photocorrosion oxidation would produce CuO which in turn consumes electrons for reduction back to Cu_2O, resulting in large dark currents in Figure 4f. As a result, we can observe that the current becomes much more negative over time in the bare Cu_2O electrode, as shown in Figure 4e. These observations together demonstrate that the $Cu_3(BTC)_2$ coating can effectively protect Cu_2O from photocorrosion oxidation and thus significantly improve the durability. The characterizations (Figure S18) also demonstrate that trace Cu(0) can be formed on the surface during the PEC process, which may contribute to the catalytic sites for CO_2 reduction; however, the excessive formation of Cu(0) at a too negative bias is detrimental to the CO_2 reduction activity of $Cu_3(BTC)_2/Cu_2O$ (Figure 4c and d).

CONCLUSION

In conclusion, we have developed a facile *in situ* growth procedure for coating the MOF material $Cu_3(BTC)_2$ on the surface of a Cu_2O photocathode. The coated MOF layer plays triple roles in PEC CO_2 reduction: (i) protecting the underlying Cu_2O from photocorrosion and helping to form trace Cu(0) species, (ii) facilitating charge separation and interfacial electron transfer to active sites, and (iii) providing active sites for catalytic CO_2 reduction. As a desirable outcome, the coating of MOF greatly enhances the performance of Cu_2O in PEC CO_2 conversion. This work not only puts forward a promising strategy for designing advanced photoelectrodes but also sheds light on the interfacial charge dynamics beneficial for efficient PEC CO_2 reduction.

ASSOCIATED CONTENT

Supporting Information

The Supporting Information is available free of charge on the ACS Publications website at DOI: 10.1021/jacs.9b06239.

Detailed experimental section, characterization methods, and additional material characterizations (PDF)

AUTHOR INFORMATION

Corresponding Authors

*gaoc@ustc.edu.cn
*qunzh@ustc.edu.cn
*yjxiong@ustc.edu.cn

ORCID

Ning Zhang: 0000-0002-0755-1708
Qun Zhang: 0000-0002-5777-9276
Junfa Zhu: 0000-0003-0888-4261
Yujie Xiong: 0000-0002-1995-8257

Author Contributions

‖X.D., R.L., S.W.: These authors contributed equally.

Notes

The authors declare no competing financial interest.

ACKNOWLEDGMENTS

This work was supported by National Key R&D Program of China (2017YFA0207301, 2016YFA0200602, 2018YFA0208702, 2017YFA0403402), NSFC (21725102, 21703220, 21573211, 21633007), CAS Key Research Program of Frontier Sciences (QYZDB-SSW-SLH018), CAS Interdisciplinary Innovation Team, Anhui Initiative in Quantum Information Technologies (AHY090200), and Anhui Provincial Natural Science Foundation (1708085QB26). SRPES experiments were performed at the Catalysis and Surface Science Endstation in NSRL in Hefei, China. We thank USTC Center for Micro- and Nanoscale Research and Fabrication for the support.

REFERENCES

(1) Michl, J. Towards an artificial leaf? *Nat. Chem.* **2011**, *3*, 268.
(2) Kim, D.; Sakimoto, K. K.; Hong, D.; Yang, P. Artificial photosynthesis for sustainable fuel and chemical production. *Angew. Chem., Int. Ed.* **2015**, *54*, 3259.
(3) Dresselhaus, M. S.; Thomas, I. L. Alternative energy technologies. *Nature* **2001**, *414*, 332.
(4) Lewis, N. S.; Nocera, D. G. Powering the planet: chemical challenges in solar energy utilization. *Proc. Natl. Acad. Sci. U. S. A.* **2006**, *103*, 15729.
(5) Rosser, T. E.; Windle, C. D.; Reisner, E. Electrocatalytic and solar-driven CO_2 reduction to CO with a molecular manganese catalyst immobilized on mesoporous TiO_2. *Angew. Chem., Int. Ed.* **2016**, *55*, 7388.
(6) White, J. L.; Baruch, M. F.; Pander Iii, J. E.; Hu, Y.; Fortmeyer, I. C.; Park, J. E.; Zhang, T.; Liao, K.; Gu, J.; Yan, Y.; Shaw, T. W.; Abelev, E.; Bocarsly, A. B. Light-driven heterogeneous reduction of carbon dioxide: photocatalysts and photoelectrodes. *Chem. Rev.* **2015**, *115*, 12888.
(7) Kumar, B.; Llorente, M.; Froehlich, J.; Dang, T.; Sathrum, A.; Kubiak, C. P. Photochemical and photoelectrochemical reduction of CO_2. *Annu. Rev. Phys. Chem.* **2012**, *63*, 541.
(8) Chu, S.; Ou, P.; Ghamari, P.; Vanka, S.; Zhou, B.; Shih, I.; Song, J.; Mi, Z. Photoelectrochemical CO_2 reduction into syngas with the metal/oxide interface. *J. Am. Chem. Soc.* **2018**, *140*, 7869.
(9) Jang, J.-W.; Cho, S.; Magesh, G.; Jang, Y. J.; Kim, J. Y.; Kim, W. Y.; Seo, J. K.; Kim, S.; Lee, K.-H.; Lee, J. S. Aqueous-solution route to zinc telluride films for application to CO_2 reduction. *Angew. Chem., Int. Ed.* **2014**, *53*, 5852.
(10) Jang, Y. J.; Jang, J.-W.; Lee, J.; Kim, J. H.; Kumagai, H.; Lee, J.; Minegishi, T.; Kubota, J.; Domen, K.; Lee, J. S. Selective CO production by Au coupled ZnTe/ZnO in the photoelectrochemical CO_2 reduction system. *Energy Environ. Sci.* **2015**, *8*, 3597.
(11) Kecsenovity, E.; Endrődi, B.; Tóth, P. S.; Zou, Y.; Dryfe, R. A. W.; Rajeshwar, K.; Janáky, C. Enhanced photoelectrochemical performance of cuprous oxide/graphene nanohybrids. *J. Am. Chem. Soc.* **2017**, *139*, 6682.
(12) Schreier, M.; Luo, J.; Gao, P.; Moehl, T.; Mayer, M. T.; Grätzel, M. Covalent immobilization of a molecular catalyst on Cu_2O photocathodes for CO_2 reduction. *J. Am. Chem. Soc.* **2016**, *138*, 1938.
(13) Grätzel, M. Photoelectrochemical cells. *Nature* **2001**, *414*, 338.
(14) Walter, M. G.; Warren, E. L.; McKone, J. R.; Boettcher, S. W.; Mi, Q.; Santori, E. A.; Lewis, N. S. Solar water splitting cells. *Chem. Rev.* **2010**, *110*, 6446.
(15) Toe, C. Y.; Zheng, Z.; Wu, H.; Scott, J.; Amal, R.; Ng, Y. H. Photocorrosion of cuprous oxide in hydrogen production: ration-

DOI: 10.1021/jacs.9b06239
J. Am. Chem. Soc. 2019, 141, 10924–10929

alising self-oxidation or self-reduction. *Angew. Chem., Int. Ed.* **2018**, *57*, 13613.
(16) Paracchino, A.; Mathews, N.; Hisatomi, T.; Stefik, M.; Tilley, S. D.; Grätzel, M. Ultrathin films on copper(I) oxide water splitting photocathodes: a study on performance and stability. *Energy Environ. Sci.* **2012**, *5*, 8673.
(17) Pan, L.; Kim, J. H.; Mayer, M. T.; Son, M.-K.; Ummadisingu, A.; Lee, J. S.; Hagfeldt, A.; Luo, J.; Grätzel, M. Boosting the performance of Cu_2O photocathodes for unassisted solar water splitting devices. *Nat. Catal.* **2018**, *1*, 412.
(18) Zhu, L.; Liu, X.-Q.; Jiang, H.-L.; Sun, L.-B. Metal-organic frameworks for heterogeneous basic catalysis. *Chem. Rev.* **2017**, *117*, 8129.
(19) Nam, D.-H.; Bushuyev, O. S.; Li, J.; De Luna, P.; Seifitokaldani, A.; Dinh, C.-T.; García de Arquer, F. P.; Wang, Y.; Liang, Z.; Proppe, A. H.; Tan, C. S.; Todorović, P.; Shekhah, O.; Gabardo, C. M.; Jo, J. W.; Choi, J.; Choi, M.-J.; Baek, S.-W.; Kim, J.; Sinton, D.; Kelley, S. O.; Eddaoudi, M.; Sargent, E. H. Metal-organic frameworks mediate cu coordination for selective CO_2 electroreduction. *J. Am. Chem. Soc.* **2018**, *140*, 11378.
(20) Li, R.; Hu, J.; Deng, M.; Wang, H.; Wang, X.; Hu, Y.; Jiang, H.-L.; Jiang, J.; Zhang, Q.; Xie, Y.; Xiong, Y. Integration of an inorganic semiconductor with a metal-organic framework: a platform for enhanced gaseous photocatalytic reactions. *Adv. Mater.* **2014**, *26*, 4783.
(21) Decoste, J. B.; Peterson, G. W.; Smith, M. W.; Stone, C. A.; Willis, C. R. Enhanced stability of Cu-BTC MOF via perfluorohexane plasma-enhanced chemical vapor deposition. *J. Am. Chem. Soc.* **2012**, *134*, 1486.
(22) DeCoste, J. B.; Peterson, G. W.; Schindler, B. J.; Killops, K. L.; Browe, M. A.; Mahle, J. J. The effect of water adsorption on the structure of the carboxylate containing metal-organic frameworks Cu-BTC, Mg-MOF-74, and UiO-66. *J. Mater. Chem. A* **2013**, *1*, 11922.
(23) Pavlishchuk, V. V.; Addison, A. W. Conversion constants for redox potentials measured versus different reference electrodes in acetonitrile solutions at 25°C. *Inorg. Chim. Acta* **2000**, *298*, 97.
(24) Dhumal, N. R.; Singh, M. P.; Anderson, J. A.; Kiefer, J.; Kim, H. J. Molecular interactions of a Cu-based metal-organic framework with a confined imidazolium-based ionic liquid: a combined density functional theory and experimental vibrational spectroscopy study. *J. Phys. Chem. C* **2016**, *120*, 3295.
(25) Todaro, M.; Alessi, A.; Sciortino, L.; Agnello, S.; Cannas, M.; Gelardi, F. M.; Buscarino, G. Investigation by Raman spectroscopy of the decomposition process of HKUST-1 upon exposure to air. *J. Spectrosc.* **2016**, *2016*, 8074297.
(26) Chang, X.; Wang, T.; Zhang, P.; Wei, Y.; Zhao, J.; Gong, J. Stable aqueous photoelectrochemical CO_2 reduction by a Cu_2O dark cathode with improved selectivity for carbonaceous products. *Angew. Chem., Int. Ed.* **2016**, *55*, 8840.
(27) Azimi, H.; Kuhri, S.; Osvet, A.; Matt, G.; Khanzada, L. S.; Lemmer, M.; Luechinger, N. A.; Larsson, M. I.; Zeira, E.; Guldi, D. M.; Brabec, C. J. Effective ligand passivation of Cu_2O nanoparticles through solid-state treatment with mercaptopropionic acid. *J. Am. Chem. Soc.* **2014**, *136*, 7233.
(28) Lee, D. Y.; Shinde, D. V.; Yoon, S. J.; Cho, K. N.; Lee, W.; Shrestha, N. K.; Han, S.-H. Cu-Based metal-organic frameworks for photovoltaic application. *J. Phys. Chem. C* **2014**, *118*, 16328.
(29) Greiner, M. T.; Helander, M. G.; Tang, W.-M.; Wang, Z.-B.; Qiu, J.; Lu, Z.-H. Universal energy-level alignment of molecules on metal oxides. *Nat. Mater.* **2012**, *11*, 76.

DOI: 10.1021/jacs.9b06239
J. Am. Chem. Soc. 2019, 141, 10924−10929